

Ab initio informed $^{20}\text{Ne}(p, p\alpha)^{16}\text{O}$ reaction elucidates the emergence of alpha clustering from chiral potentials

G. H. Sargsyan,¹ Kazuki Yoshida,² Kazuyuki Ogata,^{3,4} K. D. Launey,⁵ J. E. Escher,⁶ D. Langr,⁷ and T. Dytrych^{8,5}

¹Facility for Rare Isotope Beams, Michigan State University, East Lansing, Michigan 48824, USA

²Advanced Science Research Center, Japan Atomic Energy Agency, Tokai, Ibaraki 319-1195, Japan

³Department of Physics, Kyushu University, Fukuoka 819-0395, Japan

⁴Research Center for Nuclear Physics (RCNP), Osaka University, Ibaraki, Osaka, 567-0047, Japan

⁵Department of Physics and Astronomy, Louisiana State University, Baton Rouge, LA 70803, USA

⁶Lawrence Livermore National Laboratory, Livermore, California 94550, USA

⁷Department of Computer Systems, Faculty of Information Technology,

Czech Technical University in Prague, Prague 16000, Czech Republic

⁸Nuclear Physics Institute of the Czech Academy of Sciences, 250 68 Řež, Czech Republic

We report on the first *ab initio* informed α knock-out reaction in the intermediate-mass region, with the aim to probe the underlying chiral potential and its impact on the emergence of alpha clustering in this mass region. The theoretical predictions of the $\alpha+^{16}\text{O}$ clustering in the ^{20}Ne ground state, based on the *ab initio* symmetry-adapted no-core shell model with continuum, yield a triple differential cross section for $^{20}\text{Ne}(p, p\alpha)^{16}\text{O}$ that is in a remarkable agreement with the data. This allows us to examine predictions of surface and in-medium α -cluster features that emerge from the underlying realistic nucleon-nucleon interaction with no parameters fitted to nuclear data beyond the two-body system, and to compare these to the successful antisymmetrized molecular dynamics approach.

I. INTRODUCTION

Elucidating α clustering, along with the inter- and intra-cluster structure, is of utmost significance to further understanding dominant nuclear features relevant to processes from fusion to fission. Historically, in cross section calculations of a nuclear reaction, the effects of the intrinsic structure of the reaction fragments (or clusters) have been discussed through spectroscopic factors (SF), determined as normalization coefficients in the reaction cross sections. However, such normalization coefficients, in general, reflect any difference between the few-body theory and experiment. Alternatively, a more direct probe of the structure can be proffered by microscopic SF that are calculated from the underlying many-body theory (e.g., as done in Ref. [1]). Yet, SF, as integrals over the wavefunction, do not provide insights into the formation of alpha clusters on the surface and the role of the interior nuclear medium. Thereby, to probe α -cluster features that emerge within nuclei from the underlying nucleon-nucleon interaction derived in the framework of chiral effective field theory (EFT) [2–5] (also called “chiral potential”), here we utilize a knock-out ($p, p\alpha$) reaction, which is very sensitive to the details of alpha clustering of the target nucleus [6].

α -Cluster substructures in nuclei are extremely challenging to model, since the wavefunctions expand to large distances. This is especially difficult for *ab initio* approaches that utilize nucleon degrees of freedom and realistic interactions between the nucleons, typically, chiral potentials. Pioneering *ab initio* studies that have addressed this problem include the nuclear lattice effective field theory, used to study the energy of the Hoyle state and α - α scattering relevant to astrophysics [7–9], Green’s function Monte Carlo technique, which has been applied to the α -cluster structures of ^8Be and ^{12}C [10, 11], and

the hyperspherical harmonics method, which has been utilized for analyzing giant resonance modes in ^4He [12] (see, for example, the review [13]). Furthermore, recent advancements include α -capture reaction descriptions in the intermediate-mass region using wavefunctions from the symmetry-adapted no-core shell model (SA-NCSM) [14], studies of α clustering in even-even Be and ^{12}C isotopes using the no-core Monte Carlo shell model [15], $\alpha+\alpha$ calculations using the no-core shell model with continuum [16], as well as studies of the role of α channels using explicit continuum degrees of freedom [17, 18].

In this letter, we provide the first *ab initio* informed α knock-out reaction in the intermediate-mass region. In particular, we use the wavefunction of the target nucleus ^{20}Ne , calculated in the *ab initio* SA-NCSM, reviewed in Refs. [19, 20] and detailed below. This wavefunction accounts for the full microscopic structure of the target and when coupled to the continuum provides an $\alpha+^{16}\text{O}$ cluster wavefunction. We show that this, when used in the theory of the reaction dynamics described below, yield a triple differential cross section for $^{20}\text{Ne}(p, p\alpha)^{16}\text{O}$ that is in a remarkable agreement with the data. By doing so, we gain insights into the interior and surface α clustering in ^{20}Ne from first principles that are probed at different proton kinetic energies.

At incident energies of about 100 to 200 MeV, the distorted wave impulse approximation (DWIA) has been shown to be well suited for the analysis of ($p, p\alpha$) reactions [21]. These DWIA calculations, in which the incoming and outgoing plane waves are distorted as a result of the interaction between the reaction fragments, rely on the availability of an α cluster wavefunction. Historically, the α cluster wavefunctions have been obtained from simple Woods-Saxon potentials that are adjusted to reproduce α separation energies. In more recent studies [6], the $^{20}\text{Ne}(p, p\alpha)^{16}\text{O}$ cross sections

have been calculated with the input α cluster wavefunctions obtained from the antisymmetrized molecular dynamics (AMD) method [22–24]. Here, we utilize a parameter-free input of α cluster wavefunctions derived from SA-NCSM large-scale calculations for ^{20}Ne that use a chiral potential.

II. THEORETICAL FRAMEWORK

A. *Ab initio* SA-NCSM with continuum

We employ the *ab initio* symmetry-adapted no-core shell model (SA-NCSM) [19, 20, 25], which treats all nucleons in the system at an equal footing and admits chiral EFT interactions between the nucleons. The use of chiral EFT interactions, which are consistent with the chiral symmetry- and symmetry-breaking patterns of quantum chromodynamics, enables nuclear calculations informed by physics of two and three nucleons only. In addition, the symmetry-adapted (SA) basis in the many-body SA-NCSM approach provides solutions to otherwise infeasible ultra-large model spaces [19, 25], which are imperative for the description of challenging features in nuclei, such as clustering, collectivity, and coupling to the continuum. We note that the SA-NCSM results exactly reproduce those of the traditional NCSM [26, 27] for the same nuclear interaction. However, it utilizes the emergent symplectic symmetry $\text{Sp}(3, \mathbb{R}) \supset \text{SU}(3) \supset \text{SO}(3)$ in nuclei [25], where each $\text{Sp}(3, \mathbb{R})$ -preserving subset of basis states describes a nuclear shape and each $\text{SU}(3)$ -preserving subset informs the specific deformation. By doing so, the SA-NCSM can achieve convergence of results and describe localized α clusters with only a fraction of the corresponding NCSM space [14, 28].

Similarly to the traditional NCSM, the SA-NCSM uses a harmonic oscillator (HO) single-particle basis with frequency $\hbar\Omega$ and a model space cutoff (given by the maximum total HO excitation quanta above the valence-shell configuration), which inform the resolution and the space size in which the nucleus resides. The calculations become independent of $\hbar\Omega$ in the infinite-size model space (infinitely many HO shells), providing a parameter-free *ab initio* prediction.

The cluster wavefunction, the so-called spectroscopic amplitude (also called “reduced width amplitudes”), for the ^{20}Ne ground state is calculated through its overlap with an $\alpha + ^{16}\text{O}$ cluster state $|\Psi_{\mathbf{a}'\mathbf{a}''(I'\pi' I''\pi''); I_{n_r, \ell}}\rangle$, which is fully antisymmetrized and normalized, as detailed in Refs. [14, 29]:

$$u_{\nu I \ell}^{J^\pi}(r) = \sum_{n_r} R_{n_r, \ell}(r) \langle \Psi_{\mathbf{a}}^{J^\pi(M)} | \Psi_{\mathbf{a}'\mathbf{a}''(I'\pi' I''\pi''); I_{n_r, \ell}}^{J^\pi(M)} \rangle, \quad (1)$$

given for distance r between the center-of-mass (c.m.) of the clusters. In Eq. (1), the cluster system is defined for a channel ν , which is given by the spin and parity of each of the clusters $\nu = \{\mathbf{a}; \mathbf{a}', I'\pi', \mathbf{a}'', I''\pi''\}$ (the labels \mathbf{a} , \mathbf{a}'

and \mathbf{a}'' denote all other quantum numbers needed to fully characterize their respective states), and a partial wave ℓ , or the orbital angular momentum of the relative motion of the clusters, and has a good total angular momentum and parity, J^π , given by the coupling of the total angular momentum I of the clusters to ℓ .

$R_{n_r, \ell}(r)$ are the HO radial functions, with n_r denoting the radial HO quantum number (we note that for overlaps calculated in the SA-NCSM, $R_{n_r, \ell}$ are defined as positive at infinite distance). In this study, $\nu = \{^{20}\text{Ne}(0_{\text{gs}}^+); \alpha(0_{\text{gs}}^+), I'\pi' = 0^+, ^{16}\text{O}(0_{\text{gs}}^+), I''\pi'' = 0^+\}$, $I = 0$, and $J^\pi = 0^+$ [to simplify notations, $u_\ell(r)$ will be used henceforth].

Within a no-core shell-model framework, the $|\Psi_{^{20}\text{Ne}(0_{\text{gs}}^+)}^{J^\pi(M)}\rangle$ state of the ^{20}Ne composite system is calculated for particle laboratory coordinates. We note that, as detailed in Ref. [14], this state is exactly factorized to intrinsic and c.m. wavefunctions. The c.m. wavefunction is in the lowest HO energy and entirely integrated out in (1), yielding a translationally invariant cluster wavefunction.

At large distance r , the cluster wavefunction $u_\ell(r)$ for bound states should asymptotically approach the exact Coulomb Whittaker function, $W_{-\eta, \ell + \frac{1}{2}}$:

$$ru_\ell(r) \rightarrow C_\ell W_{-\eta, \ell + \frac{1}{2}}(2kr), \quad (2)$$

where $k = \sqrt{2\mu B}/\hbar$, with B being the cluster separation energy and μ the reduced mass, η is the Sommerfeld parameter, $\eta = \mu Z' Z'' / \hbar^2 k$, with Z' and Z'' being the proton numbers of each of the clusters. The C_ℓ coefficient is called the asymptotic normalization coefficient (ANC). In this study, we use the SA-NCSM cluster wavefunction of Eq. (1) in the interior and the exact Coulomb function at large distances, both of which are matched using logarithmic derivatives within an R-matrix framework [30], as often done in many-body approaches (see, e.g., [14, 16, 17, 31]). This, in turn, determines the ANC. While various methods exist for calculating ANCs (see, e.g., [32–34]), we use the prescription of Ref. [1], which utilizes (2), while retaining the microscopically calculated SF, the norm of $u_\ell(r)$ of Eq. (1). This prescription benefits from the use of SA-NCSM to calculate the interior wavefunction, as sufficiently large model spaces are critical to achieve accurate descriptions in the interior.

In this study, the fully microscopic wavefunction of the ^{20}Ne ground state is calculated using the NNLO_{opt} NN chiral potential [35] in the *ab initio* SA-NCSM many-body approach, which has yielded energy spectra and observables (radii, quadrupole moments, $E2$ transitions, and charge form factors) in close agreement with experiment [19, 20, 25]. The NNLO_{opt} is fitted only to NN scattering phase shifts and properties of the deuteron and is used without three-nucleon forces, which have been shown to contribute minimally to the three- and four-nucleon binding energies [35]. Furthermore, the NNLO_{opt} NN potential has been found to reproduce various observables and yield results equivalent to those obtained from chiral potentials that require three-nucleon

forces. These observables include the ^4He electric dipole polarizability [36]; the challenging analyzing power for elastic proton scattering on ^4He , ^{12}C , and ^{16}O [37]; along with $B(E2)$ transition strengths for $^{21,28}\text{Mg}$ and ^{21}F [38, 39] in the SA-NCSM without effective charges, as well as collective and dynamical observables for ^{40}Ca [40, 41] and ^{48}Ti [20].

B. Knock-out reaction theory

We follow the distorted-wave impulse approximation (DWIA) [21, 42, 43] reaction analysis for $^{20}\text{Ne}(p, p\alpha)^{16}\text{O}$ of Ref. [6]. Namely, the triple-differential cross section with respect to the kinetic energy of the emitted proton T_p^L , emission angle of the proton Ω_p^L , and the α emission angle Ω_α^L is given by

$$\frac{d^3\sigma}{dT_p^L d\Omega_p^L d\Omega_\alpha^L} = F_{\text{kin}} C_0 \frac{d\sigma_{p\alpha}}{d\Omega_{p\alpha}} |\bar{T}|^2, \quad (3)$$

where the superscript L indicates that the quantities are evaluated in the laboratory frame of the reaction. F_{kin} consists of the phase volume factor and the Jacobian from the center-of-mass frame to the laboratory frame. $d\sigma_{p\alpha}/d\Omega_{p\alpha}$ is the p - α elementary cross section. A constant C_0 contains physics constants and factors related to the p - α elementary process. The TDX (3) depends on the so-called reduced transition matrix \bar{T} of the DWIA framework using the cluster wavefunction u_0 , and similarly to Eq. (6) of Ref. [6] is given by

$$\bar{T} = \int d\mathbf{r} F(\mathbf{r}) u_{\ell=0}(r) Y_{00}(\hat{\mathbf{r}}), \quad (4)$$

assuming $\ell = 0$ based on the single-peak shape of the experimental TDX. $F(r)$ is determined by the incoming and outgoing distorted waves as defined in Eq. (7) in Ref. [6].

The DWIA calculations are performed using PIKOE [44]. To provide a level of specificity for completeness, we note that except the cluster wavefunction, all the inputs for the DWIA calculations are the same as in Ref. [6]. In particular, the interactions between all pairs of reaction fragments, called optical potentials, are adopted as following: For the proton scattering, the EDAD1 global optical potential of the Dirac phenomenology [45–47] is adopted and the α - ^{16}O optical potential by Michel [48] is adopted for the α scattering wave in the final state. We also show results that use the global proton optical potential by Koning and Delaroche [49]. The p - α elementary cross section, $d\sigma_{p\alpha}/d\Omega_{p\alpha}$, is calculated by the folding model [50] using the Melbourne g -matrix interaction. See Sec. II of Refs. [6, 43] for more details of the reaction framework and Eqs. (4) and (3).

In Sec. III, the $^{20}\text{Ne}(p, p\alpha)^{16}\text{O}$ TDX is compared with the experimental data by Carey et al. [51]. In the experiment, the emission angle of the proton is fixed at $\theta_p^L = 70^\circ$ and $\phi_p^L = 180^\circ$, and the α emission angle is

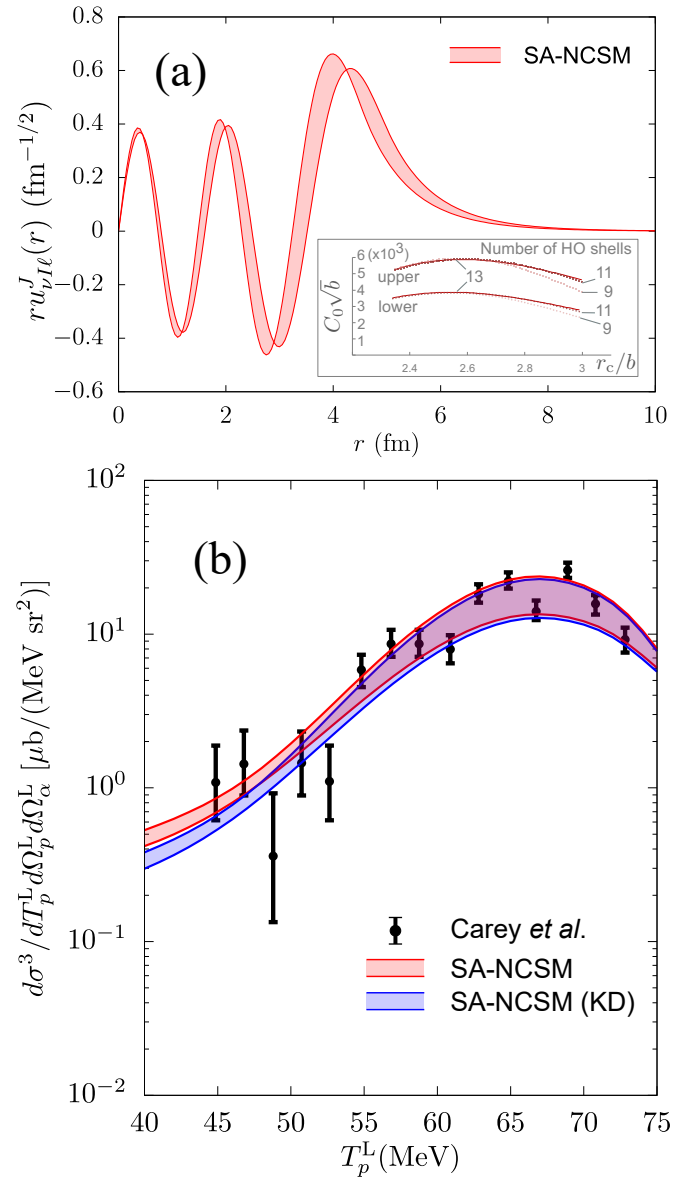


FIG. 1. (a) $\alpha+^{16}\text{O}$ S partial wave for the ^{20}Ne ground state, calculated in the *ab initio* symmetry-adapted no-core shell model with the NNLO_{opt} NN chiral potential in 13 HO shells, with many-body model uncertainties (red band). Inset: ANC C_0 vs. the channel radius r_c (relative to the HO length b), shown for model spaces of 9, 11, and 13 HO shells. (b) Triple differential cross sections for the α knock-out reaction $^{20}\text{Ne}(p, p\alpha)^{16}\text{O}$ vs. the proton kinetic energy using the cluster wavefunction shown in (a), and compared to the experiment of Ref. [51] (labeled as “Carey et al.”). “SA-NCSM” shows the result using the EDAD1 optical potential for the proton scattering (red band), while “SA-NCSM (KD)” uses the Koning-Delaroche optical potential (blue band). See text for details.

fixed at $\theta_\alpha^L = 46.3^\circ$ and $\phi_\alpha^L = 0^\circ$. The theoretical calculations are performed according to the experimental setup. With this kinematics, the TDX distribution with respect to the kinetic energy of the emitted proton T_p is measured. At around $T_p = 67$ MeV, the so-called recoil-less condition is achieved and the TDX is peaked, reflecting

the $\ell = 0$ nature of the α cluster.

III. RESULTS AND DISCUSSIONS

We report on the first *ab initio* informed α knock-out reaction for the intermediate-mass ^{20}Ne nucleus, which yields a triple differential cross section for $^{20}\text{Ne}(p, p\alpha)^{16}\text{O}$ that reproduces the experimental data of Ref. [51] (Fig. 1). The NNLO_{opt} chiral potential is used in the SA-NCSM many-body approach to calculate the ^{20}Ne 0^+ ground state, which in turn is projected on the $\alpha+^{16}\text{O}$ S partial wave to compute $u_0(r)$ according to Eq. (1) (Fig. 1a). With $u_0(r)$ supplied to the few-body theoretical framework of the knock-out reaction dynamics outlined in Sec. IIB, the agreement to data is remarkable given that the α -cluster features in ^{20}Ne emerge from the underlying chiral potential that is fitted to only two-nucleon systems, with no additional parameters to tweak. Furthermore, the use of the global proton optical potential by Koning and Delaroche [49] yields only marginal differences at low proton kinetic energies T_p^L , as shown in Fig. 1b. This makes the output being practically independent from the specific model for the proton optical potential. Based on this, the results reported henceforth utilize the EDAD1 global optical potential used in Ref. [6].

In particular, we adopt the $u_0(r)$ $\alpha+^{16}\text{O}$ cluster wavefunction for the ^{20}Ne ground state that have been reported and detailed in Ref. [14]. We note that excitations of α are not considered given the 20.21-MeV first excited state in ^4He . In addition, since the NNLO_{opt} yields a ^4He wavefunction that is 90-95% in the spin-zero s -shell configuration, using this configuration only results in an approximation that practically does not affect the final results. To provide parameter-free input to the $(p, p\alpha)$ cross section, we ensure convergence of the ANC coefficients for $u_0(r)$ in the limit of the infinite-size model space. This is based on an important feature we find here for the ANC, namely, while the ANC coefficients slightly increase with the model space size for $\hbar\Omega = 11$ MeV, they decrease for $\hbar\Omega = 13$ MeV, providing a stringent lower and upper limit for this quantity, $C_0 = 3.7(7) \times 10^3 \text{ fm}^{-1/2}$. This is consistent with the value reported in Ref. [14] for the range of $\hbar\Omega = 13$ -17 MeV in 13 HO shells, while yielding uncertainty that is smaller by a factor of two. In addition, Ref. [14] has shown that with decreasing $\hbar\Omega$, at about $\hbar\Omega = 13$ MeV the ANCs become independent from the r_c channel radius, the radius at which Eq. (2) is calculated (see Fig. 5 of Ref. [14]). Indeed, the independence from r_c is evident by the flat regions in C_0 across r_c , shown in the inset of Fig. 1, which improves with larger model spaces (naturally, for r_c smaller than the effective range of the interaction C_0 decreases, as manifested around $r_c \lesssim 2.5b$, where $b = \sqrt{\frac{\hbar}{m\Omega}}$ is the HO length, with m being the average nucleon mass).

Based on this estimate for the ANC, we use clus-

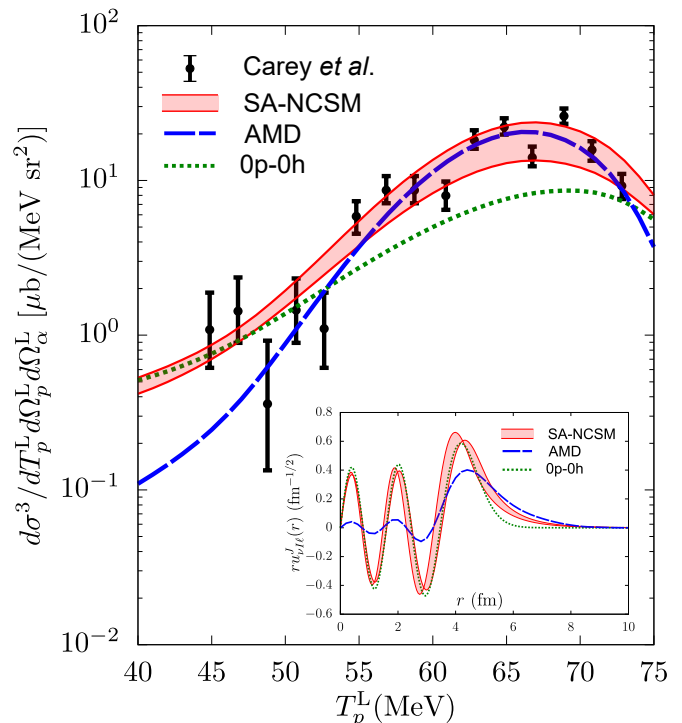


FIG. 2. Same as Fig. 1b, but including the cross section using the AMD cluster wavefunction (dashed blue) and the 0p-0h contribution (dotted green) of the upper-limit SA-NCSM cluster wavefunction. Inset: same as Fig. 1a, but including the corresponding cluster wavefunctions.

ter wavefunctions calculated in the SA-NCSM in 13 HO shells for $\hbar\Omega = 11$ MeV as an upper limit and for $\hbar\Omega = 13$ MeV as a lower limit (the use of “upper limit” reflects the ANC upper limit, but also corresponds to the upper bound in the TDX uncertainty band of Fig. 1b, similarly, “lower limit” corresponds to the ANC and TDX lower bounds). These two limits define the many-body model uncertainties. We also note that using these limits, the SA-NCSM calculations yield a ^{20}Ne ground-state charge radius¹ of 2.94(9) fm, in agreement with the experimental value of 3.0055(21) fm [53]. As clearly evident in Fig. 1a, the cluster wavefunction reveals α clustering around the ^{16}O surface but also, to a lesser but comparable extent, within the ^{16}O interior. Since wavefunctions are not observables and the ^{20}Ne ground state ANC have not yet been deduced experimentally, the $(p, p\alpha)$ data is an ideal opportunity to examine emergent clustering features. These are also compared in Fig. 2 to the outcomes of the successful AMD approach and to the case of eliminating collective and continuum correlations, that is, valence-shell calculations, as discussed below.

The peripheral behavior of the $(p, p\alpha)$ reaction, that

¹ We calculate the charge radius from the point-proton rms radius using the constants $R_p = 0.84184(67)$ fm [52] and $R_n^2 = -0.1149(27)$ fm² [53], plus relativistic and spin-orbit corrections as detailed in [54].

is, the extent to which the reaction is sensitive to the surface region only, is mainly determined by the α emission energy, T_α^L , and the absorption effect of the emitted α (which is described by the imaginary part of the α optical potential). Since for a given kinetic energy T_p^L of the emitted proton, $T_p^L + T_\alpha^L$ are constrained by the beam energy, in addition to the α separation energy and the recoil of the reaction residues, higher proton kinetic energies T_p^L imply smaller T_α^L . Of a particular interest is the maximum of the knock-out cross section, which occurs at $T_p^L \sim 67$ MeV. It corresponds to a zero recoil momentum \mathbf{k} of the reaction residues and probes surface α clustering. One can understand this in the simple framework of a plane-wave (PW) approximation, where Eq. (4) becomes $\bar{T}_{PW} = \int d\mathbf{r} e^{i\mathbf{k}\cdot\mathbf{r}} u_0(\mathbf{r})$ with $|\bar{T}_{PW}(k=0)|^2 = |\int d\mathbf{r} u_0(\mathbf{r})|^2$, which is given by the area under the cluster wavefunctions in the inset of Fig. 2. Since the contribution from the interior peaks practically cancels, the area is indeed determined from the surface peak. Therefore, the $(p, p\alpha)$ cross section around $T_p^L \sim 67$ MeV is determined by the surface region of $u_0(r)$.

Interestingly, while the AMD approach yields overall surface clustering features and wavefunction tail similar to what the SA-NCSM with NNLO_{opt} reveals, the taller and more compact surface peak for SA-NCSM yields practically the same area beneath, as the shorter but wider peak in the AMD approach (Fig. 2). In addition, the surface peak location for the AMD and SA-NCSM (upper limit) practically coincide (4.4 fm for AMD and 4.32 fm for SA-NCSM). Further accounting for the absorption effect of the emitted α , this results in a good agreement of both AMD and SA-NCSM approaches to the data around $T_p^L \sim 67$ MeV that have small uncertainties. Furthermore, we consider only the 0-particle-0-hole (0p-0h) contribution of the SA-NCSM cluster wavefunction (upper limit) as input to the cross section, that is, an alpha particle in the valence shell in ^{20}Ne . In this case, the narrower surface peak (see the green dotted curve in the inset of Fig. 2) largely underestimates the cross section. This emphasizes the critical role of correlations beyond the 0p-0h contribution such as collective correlations and coupling to the continuum that enter the entire SA-NCSM cluster wavefunction, for reproducing the cross section.

Similarly, low T_p^L proton kinetic energies probe – to a certain extent – higher-energy alpha particles that leave the nuclear interior. Even though the scattering waves have a smaller amplitude in the interior region due to the absorption effect arising from the imaginary part of the optical potential and suppress the reaction sensitivity to this region, the larger difference of the interior AMD and SA-NCSM wavefunctions lead to some noticeable deviations (at a logarithmic scale) at low T_p^L energies, in both the height and the shape of the TDX tail (Fig. 2). However, in this region, the 0p-0h contribution yields a cross section comparable with that of the entire SA-NCSM cluster wavefunction, likely as a result of the similar wavefunction behavior at short distances

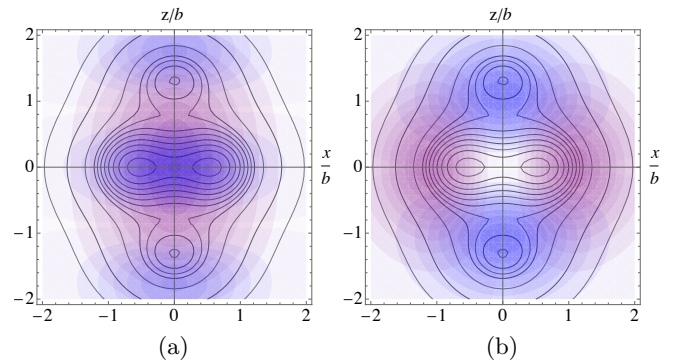


FIG. 3. Intrinsic one-body density profile for ^{20}Ne (black contours) in the $\{x, z\}$ plane (relative to b), shown with the contributions from the lowest five most dominant natural single-particle orbitals with (a) positive parity: s -shell dominated (purple) and sd -shell dominated (blue), as well as (b) negative parity: p -shell dominated with HO excitations mainly along the z axis (blue) and x axis (purple).

(Fig. 2, inset). In particular, the NNLO_{opt} chiral potential suggests strong mixing between the clusters within the nuclear medium predominantly arising from 0p-0h configurations, as discussed next. With such mixing, the *ab initio* informed cross section agrees with the measurements below $T_p^L \sim 55$ MeV within about 1σ (Fig. 1b).

To understand the cluster features within the nuclear medium, as emerging from the NNLO_{opt} chiral potential, we examine the intrinsic (*body-fixed*) one-body density (Fig. 3), which informs about the probability of finding a single particle at a given position within the ^{20}Ne ground-state wavefunction. The eigenvectors of the one-body density matrix are often referred to as natural orbitals. We find that only five spatial natural orbitals are largely occupied (with maximum of four particles per orbital, two protons and two neutrons with spin up and down). Each of these natural orbitals contributes 19.9% to the overall occupancy and is calculated as an eigenvector of the one-body density matrix for the SA-NCSM ^{20}Ne ground state using basis configurations with probability amplitudes more than 2%. Clearly, the natural orbitals with dominant p -shell and sd -shell contributions to the density (blue shades in Fig. 3) are important in shaping the α surface peak. However, among the two, the positive-parity natural orbital contributes significantly to both the surface peak and the interior, and thus highly overlaps with the cluster in the center described by a dominant s -shell configuration (Fig. 3a).

In short, we present the first study that probes details of emergent clustering features from chiral potentials in the intermediate-mass region, including surface α clustering and cluster mixing. We show that the $\alpha+^{16}\text{O}$ cluster wavefunction from the SA-NCSM with NNLO_{opt}, coupled with proton and alpha optical potentials that enter the few-body theory, reproduce within the statistics the triple differential cross section for the α knock-out reaction on ^{20}Ne . In particular, we show that, in the region

around the maximum cross section that probes surface α clustering, the SA-NCSM approach yields similar cluster features to those of AMD, confirming the critical need for collective correlations and coupling to the continuum for reproducing the cross section. Whereas within the nuclear medium, the NNLO_{opt} chiral potential suggests strong mixing between the clusters and largely overlapping clusters. The remarkable agreement to experiment further validates the properties of the NNLO_{opt} chiral potential for predicting collective and clustering features in the intermediate-mass region, and confirms the significance of the *ab initio* SA-NCSM approach that is capable to facilitate the relevant many-body configurations and, thereby, to describe localized clustering from first principles beyond the lightest nuclear systems. This work paves the way toward using cluster wavefunctions derived from *ab initio* SA-NCSM calculations as input to α knock-out cross sections, as well as to inform and support $(p,\rho\alpha)$ measurements in the intermediate- and medium-mass region.

IV. ACKNOWLEDGMENTS

This work was supported by the U.S. Department of Energy (DE-SC0023532, DE-FG02-93ER40756), as well as in part by the U.S. National Science Foundation (PHY-2209060) and the Czech Science Foundation (22-14497S). This work is also supported in part by Grant-in-Aid for Scientific Research (No. JP20K14475, and No. JP21H04975) from Japan Society for the Promotion of Science (JSPS). This material is based upon work supported by the U.S. Department of Energy, Office of Science, Office of Nuclear Physics, under the FRIB Theory Alliance award DE-SC0013617. This work was performed in part under the auspices of the U.S. Department of Energy by Lawrence Livermore National Laboratory under Contract DE-AC52-07NA27344, with support from the Laboratory Directed Research and Development Program, Projects 19-ERD-017 and 24-ERD-023. This work benefited from high performance computational resources provided by LSU (www.hpc.lsu.edu), the National Energy Research Scientific Computing Center (NERSC), a U.S. Department of Energy Office of Science User Facility at Lawrence Berkeley National Laboratory operated under Contract No. DE-AC02-05CH11231, as well as the Frontera computing project at the Texas Advanced Computing Center, made possible by National Science Foundation award OAC-1818253.

-
- [1] G. H. Sargsyan, K. D. Launey, R. M. Shaffer, S. T. Marley, N. Dudeck, A. Mercenne, T. Dytrych, and J. P. Draayer, Ab initio single-neutron spectroscopic overlaps in lithium isotopes, *Phys. Rev. C* **108**, 054303 (2023).
 - [2] P. F. Bedaque and U. van Kolck, Effective field theory for few-nucleon systems, *Annu. Rev. Nucl. Part. Sci.* **52**, 339 (2002).
 - [3] E. Epelbaum, A. Nogga, W. Glöckle, H. Kamada, U.-G. Meißner, and H. Witala, Three-nucleon forces from chiral effective field theory, *Phys. Rev. C* **66**, 064001 (2002).
 - [4] D. R. Entem and R. Machleidt, *Phys. Rev. C* **68**, 041001 (2003).
 - [5] E. Epelbaum, *Prog. Part. Nucl. Phys.* **57**, 654 (2006).
 - [6] K. Yoshida, Y. Chiba, M. Kimura, Y. Taniguchi, Y. Kanada-En'yo, and K. Ogata, Quantitative description of the $^{20}\text{Ne}(p,\rho\alpha)^{16}\text{O}$ reaction as a means of probing the surface α amplitude, *Phys. Rev. C* **100**, 044601 (2019).
 - [7] E. Epelbaum, H. Krebs, D. Lee, and U.-G. Meißner, *Phys. Rev. Lett.* **106**, 192501 (2011).
 - [8] S. Elhatisari, D. Lee, G. Rupak, E. Epelbaum, et al., Ab initio alpha-alpha scattering, *Nature* **528**, 111 (2015).
 - [9] S. Elhatisari, E. Epelbaum, H. Krebs, T. A. Lähde, D. Lee, N. Li, B.-n. Lu, U.-G. Meißner, and G. Rupak, Ab initio calculations of the isotopic dependence of nuclear clustering, *Phys. Rev. Lett.* **119**, 222505 (2017).
 - [10] R. B. Wiringa, S. C. Pieper, J. Carlson, and V. R. Pandharipande, Quantum Monte Carlo calculations of $A = 8$ nuclei, *Phys. Rev. C* **62**, 014001 (2000).
 - [11] J. Carlson, S. Gandolfi, F. Pederiva, S. C. Pieper, R. Schiavilla, K. E. Schmidt, and R. B. Wiringa, Quantum monte carlo methods for nuclear physics, *Rev. Mod. Phys.* **87**, 1067 (2015).
 - [12] S. Bacca, N. Barnea, W. Leidemann, and G. Orlandini, Isoscalar Monopole Resonance of the Alpha Particle: A Prism to Nuclear Hamiltonians, *Phys. Rev. Lett.* **110**, 042503 (2013).
 - [13] M. Freer, H. Horiuchi, Y. Kanada-En'yo, D. Lee, and U.-G. Meißner, Microscopic clustering in light nuclei, *Rev. Mod. Phys.* **90**, 035004 (2018).
 - [14] A. C. Dreyfuss, K. D. Launey, J. E. Escher, G. H. Sargsyan, R. B. Baker, T. Dytrych, and J. P. Draayer, Clustering and α -capture reaction rate from ab initio symmetry-adapted descriptions of ^{20}Ne , *Phys. Rev. C* **102**, 044608 (2020).
 - [15] T. Otsuka, T. Abe, T. Yoshida, Y. Tsunoda, N. Shimizu, N. Itagaki, Y. Utsuno, J. Vary, P. Maris, and H. Ueno, α -clustering in atomic nuclei from first principles with statistical learning and the hoyle state character, *Nature Communications* **13**, 2234 (2022).
 - [16] K. Kravvaris, S. Quaglioni, G. Hupin, and P. Navrátil, Ab initio framework for nuclear scattering and reactions induced by light projectiles, *Physics Letters B* **856**, 138930 (2024).
 - [17] A. Mercenne, N. Michel, and M. Płoszajczak, Gamow shell model description of $^4\text{He}(d,d)$ elastic scattering reactions, *Phys. Rev. C* **99**, 044606 (2019).
 - [18] J. P. L. Fernandez, N. Michel, M. Płoszajczak, and A. Mercenne, Description of ^7Be and ^7Li within the gamow shell model, *Phys. Rev. C* **108**, 044616 (2023).
 - [19] K. D. Launey, T. Dytrych, and J. P. Draayer, Symmetry-guided large-scale shell-model theory, *Prog. Part. Nucl.*

- Phys. **89**, 101 (review) (2016).
- [20] K. D. Launey, A. Mercenne, and T. Dytrych, Nuclear dynamics and reactions in the *ab initio* symmetry-adapted framework, *Annu. Rev. Nucl. Part. Sci.* **71**, 253 (2021).
- [21] N. S. Chant and P. G. Roos, Distorted-wave impulse-approximation calculations for quasifree cluster knockout reactions, *Phys. Rev. C* **15**, 57 (1977).
- [22] Y. Kanada-En'yo and H. Horiuchi, Clustering in yrast states of ^{20}Ne studied with antisymmetrized molecular dynamics, *Progress of Theoretical Physics* **93**, 115 (1995).
- [23] Y. Kanada-En'yo, H. Horiuchi, and A. Ono, Structure of Li and Be isotopes studied with antisymmetrized molecular dynamics, *Phys. Rev. C* **52**, 628 (1995).
- [24] Y. Kanada-En'yo, *Phys. Rev. Lett.* **81**, 5291 (1998).
- [25] T. Dytrych, K. D. Launey, J. P. Draayer, D. J. Rowe, J. L. Wood, G. Rosensteel, C. Bahri, D. Langr, and R. B. Baker, Physics of nuclei: Key role of an emergent symmetry, *Phys. Rev. Lett.* **124**, 042501 (2020).
- [26] P. Navrátil, J. P. Vary, and B. R. Barrett, Properties of ^{12}C in the *Ab Initio* Nuclear Shell Model, *Phys. Rev. Lett.* **84**, 5728 (2000).
- [27] B. Barrett, P. Navrátil, and J. Vary, *Prog. Part. Nucl. Phys.* **69**, 131 (2013).
- [28] G. H. Sargsyan, K. D. Launey, M. T. Burkey, A. T. Gallant, N. D. Scielzo, G. Savard, A. Mercenne, T. Dytrych, D. Langr, L. Varriano, B. Longfellow, T. Y. Hirsh, and J. P. Draayer, Impact of clustering on the ^8Li β decay and recoil form factors, *Phys. Rev. Lett.* **128**, 202503 (2022).
- [29] Y. Suzuki and K. T. Hecht, Symplectic and Cluster Excitations in Nuclei: Evaluation of interaction matrix elements, *Nucl. Phys. A* **455**, 315 (1986).
- [30] P. Descouvemont and D. Baye, *Rep. Prog. Phys.* **73**, 3 (2010).
- [31] I. Brida, S. C. Pieper, and R. B. Wiringa, Quantum Monte Carlo calculations of spectroscopic overlaps in $A \leq 7$ nuclei, *Phys. Rev. C* **84**, 024319 (2011).
- [32] C. R. Brune, Alternative parametrization of R -matrix theory, *Physical Review C* **66**, 044611 (2002).
- [33] K. M. Nollett and R. B. Wiringa, Asymptotic normalization coefficients from *ab initio* calculations, *Phys. Rev. C* **83**, 041001 (2011).
- [34] N. K. Timofeyuk, Overlap functions, spectroscopic factors, and asymptotic normalization coefficients generated by a shell-model source term, *Phys. Rev. C* **81**, 064306 (2010).
- [35] A. Ekström, G. Baardsen, C. Forssén, G. Hagen, M. Hjorth-Jensen, G. R. Jansen, R. Machleidt, W. Nazarewicz, *et al.*, An optimized chiral nucleon-nucleon interaction at next-to-next-to-leading order, *Phys. Rev. Lett.* **110**, 192502 (2013).
- [36] R. B. Baker, K. D. Launey, S. Bacca, N. N. Dinur, and T. Dytrych, Benchmark calculations of electromagnetic sum rules with a symmetry-adapted basis and hyperspherical harmonics, *Phys. Rev. C* **102**, 014320 (2020).
- [37] M. Burrows, C. Elster, S. P. Weppner, K. D. Launey, P. Maris, A. Nogga, and G. Popa, *Ab initio* folding potentials for nucleon-nucleus scattering based on no-core shell-model one-body densities, *Phys. Rev. C* **99**, 044603 (2019).
- [38] P. Ruotsalainen, J. Henderson, G. Hackman, G. H. Sargsyan, K. D. Launey, *et al.*, Isospin symmetry in $B(E2)$ values: Coulomb excitation study of ^{21}Mg , *Phys. Rev. C* **99**, 051301 (2019).
- [39] J. Williams, G. C. Ball, A. Chester, T. Domingo, A. B. Garnsworthy, G. Hackman, J. Henderson, R. Henderson, R. Krücken, A. Kumar, K. D. Launey, J. Measures, O. Paetkau, J. Park, G. H. Sargsyan, J. Smallcombe, P. C. Srivastava, K. Starosta, C. E. Svensson, K. Whitmore, and M. Williams, Structure of ^{28}Mg and influence of the neutron *pf* shell, *Phys. Rev. C* **100**, 014322 (2019).
- [40] M. Burrows *et al.*, Response functions and giant monopole resonances for light to medium-mass nuclei from the *ab initio* symmetry-adapted no-core shell model, arXiv:2312.09782 10.48550/arXiv.2312.09782 (2024).
- [41] R. B. Baker, C. Elster, T. Dytrych, and K. D. Launey, *Ab initio* leading order effective potential for elastic proton scattering based on the symmetry-adapted no-core shell model, *Phys. Rev. C* **110**, 034605 (2024).
- [42] N. S. Chant and P. G. Roos, Spin orbit effects in quasifree knockout reactions, *Phys. Rev. C* **27**, 1060 (1983).
- [43] T. Wakasa, K. Ogata, and T. Noro, Proton-induced knockout reactions with polarized and unpolarized beams, *Prog. Part. Nucl. Phys.* **96**, 32 (2017).
- [44] K. Ogata, K. Yoshida, and Y. Chazono, pikoe: A computer program for distorted-wave impulse approximation calculation for proton induced nucleon knockout reactions, *Comput. Phys. Commun.* **297**, 109058 (2024).
- [45] S. Hama, B. C. Clark, E. D. Cooper, H. S. Sherif, and R. L. Mercer, Global Dirac optical potentials for elastic proton scattering from heavy nuclei, *Phys. Rev. C* **41**, 2737 (1990).
- [46] E. D. Cooper, S. Hama, B. C. Clark, and R. L. Mercer, Global Dirac phenomenology for proton-nucleus elastic scattering, *Phys. Rev. C* **47**, 297 (1993).
- [47] E. D. Cooper, S. Hama, and B. C. Clark, Global Dirac optical potential from helium to lead, *Phys. Rev. C* **80**, 034605 (2009).
- [48] F. Michel, J. Albinski, P. Belery, T. Delbar, G. Grégoire, B. Tasiaux, and G. Reidemester, Optical model description of $\alpha+^{16}\text{O}$ elastic scattering and alpha-cluster structure in ^{20}Ne , *Phys. Rev. C* **28**, 1904 (1983).
- [49] A. Koning and J. Delaroche, Local and global nucleon optical models from 1 keV to 200 MeV, *Nucl. Phys. A* **713**, 231 (2003).
- [50] M. Toyokawa, K. Minomo, and M. Yahiro, Mass-number and isotope dependence of local microscopic optical potentials for polarized proton scattering, *Phys. Rev. C* **88**, 054602 (2013).
- [51] T. A. Carey, P. G. Roos, N. S. Chant, A. Nadasen, and H. L. Chen, Alpha-particle spectroscopic strengths using the $(p,p\alpha)$ reaction at 101.5 MeV, *Phys. Rev. C* **29**, 1273 (1984).
- [52] R. Pohl, A. Antognini, F. Nez, F. D. Amaro, F. Biraben, J. M. Cardoso, D. S. Covita, A. Dax, S. Dhawan, L. M. Fernandes, *et al.*, The size of the proton, *nature* **466**, 213 (2010).
- [53] I. Angeli and K. Marinova, Table of experimental nuclear ground state charge radii: An update, *Atomic Data and Nuclear Data Tables* **99**, 69 (2013).
- [54] S. Bacca, N. Barnea, and A. Schwenk, Matter and charge radius of ^6He in the hyperspherical-harmonics approach, *Phys. Rev. C* **86**, 034321 (2012).